Site Characterization for CO_2 Geologic Storage and Vice Versa: The Frio Brine Pilot, Texas, USA as a Case Study

Christine Doughty, Barry Freifeld, and Robert Trautz

Lawrence Berkeley National Laboratory
Earth Sciences Division
1 Cyclotron Rd.
Berkeley, CA 94720

Abstract Careful site characterization is critical for successful geologic storage of carbon dioxide (CO_2) because of the many physical and chemical processes impacting CO_2 movement and containment under field conditions. Traditional site characterization techniques such as geological mapping, geophysical imaging, well logging, core analyses, and hydraulic well testing provide the basis for judging whether or not a site is suitable for CO_2 storage. However, only through the injection and monitoring of CO_2 itself can the coupling between buoyancy flow, geologic heterogeneity, and history-dependent multi-phase flow effects be observed and quantified. CO_2 injection and monitoring can therefore provide a valuable addition to the site-characterization process. Additionally, careful monitoring and verification of CO_2 plume development during the early stages of commercial operation should be performed to assess storage potential and demonstrate permanence. The Frio brine pilot, a research project located in Dayton, Texas (USA) is used as a case study to illustrate the concept of an iterative sequence in which traditional site characterization is used to prepare for CO_2 injection and then CO_2 injection itself is used to further site-characterization efforts, constrain geologic storage potential, and validate understanding of geochemical and hydrological processes. At the Frio brine pilot, in addition to traditional site-characterization techniques, CO_2 movement in the subsurface is monitored by sampling fluid at an observation well, running CO_2-saturation-sensitive well logs periodically in both injection and observation wells, imaging with crosswell seismic in the plane between the injection and observation wells, and obtaining vertical seismic profiles to monitor the CO_2 plume as it migrates beyond the immediate vicinity of the wells. Numerical modeling plays a central role in integrating geological, geophysical, and hydrological field observations.

Keywords Geologic carbon dioxide storage · Site characterization · Multi-phase flow · Numerical modeling · Frio Formation

C. Doughty (✉) · B. M. Freifeld · R. C. Trautz
Earth Sciences Division,
Lawrence Berkeley National Laboratory,
#1 Cyclotron Road, MS 90-1116,
Berkeley, CA 94720, USA
e-mail: cadoughty@lbl.gov

Introduction

Successful geologic storage of CO_2 requires thorough site characterization, especially for storage in saline formations that have not previously been considered an economic resource. It is important to understand the processes and mechanisms by which CO_2 is transported, in light of its low density and viscosity compared to brine, and the diverse geochemical processes that can occur. Traditional site characterization techniques, such as geological mapping, geophysical imaging, well logging, core analyses, and hydraulic well testing form the foundation for assessing site suitability. However, the injection and monitoring of CO_2 itself provides a wealth of additional information, illustrating the coupling between buoyancy flow, geologic heterogeneity, and history-dependent multi-phase flow effects, factors which may ultimately determine the viability of a potential storage site.

We therefore recommend that after traditional site characterization activities (e.g., geologic, geophysical, and hydraulic testing) have been used to assess site suitability for subsurface storage of CO_2, reservoir models be reassessed

and updated using data collected during initial CO_2 injection. This initial injection of CO_2 can either be considered part of the site-characterization process, or may be the initial phase of commercial utilization of the storage reservoir. Uncertainty in the estimates for ultimate storage efficiency and plume spread can be reduced through the use of the multi-phase transport and geochemical data obtained. Because of the complexities associated with multi-phase, multi-component flow, we also recommend that a reservoir model be developed to simulate the principle storage processes in conjunction with site characterization, to facilitate integrating disparate field observations and synthesizing understanding of subsurface processes.

The procedure of adapting a model as new information is acquired is very common in the petroleum and geothermal industries and is generally called history matching. Ongoing model development in conjunction with monitoring is also part of the procedure specified by the Intergovernmental Panel on Climate Change for estimating emissions from CO_2 storage sites (IPCC 2005), This paper describes the use of the Frio brine pilot, a research project involving a small-scale CO_2 injection test conducted at the South Liberty field, in Dayton, Texas (USA), as a case study to illustrate the concept of an iterative sequence in which traditional site characterization is used to prepare for CO_2 injection and then CO_2 injection itself is used to further site-characterization efforts, constrain geologic storage potential, and validate our understanding of geochemical and hydrological processes.

The paper is organized as follows. First, the subsurface flow and transport processes relevant for geologic storage of CO_2 are reviewed, and recommended site-characterization activities for each process are presented. Next, the Frio brine pilot is described, with particular emphasis on integrating data obtained using traditional site-characterization methods with the additional information collected during the CO_2 injection and monitoring. Finally, the broader applicability of the key findings from the Frio brine pilot is discussed, followed by concluding remarks.

Subsurface flow and transport processes in geologic storage and recommended site-characterization activities

Fundamentally, site characterization must shed light on two features of the subsurface: its capacity to accept a large quantity of CO_2, thus demonstrating the economic feasibility of the project, and its ability to effectively store the CO_2 for a long time. There are three basic requirements for good storage capacity. The first requirement is adequate connected porosity, which can be assessed from well logs, core analyses, and hydraulic tests. Multi-well tracer testing can also be used to infer connected porosity, but it is expensive and is not typically employed as a site-characterization technique. The second requirement is that the density of the CO_2 be large enough to make storage economical. Density increases greatly as CO_2 makes a transition from gaseous to supercritical conditions when pressure and temperature exceed 73.8 bars and 31°C, respectively. Thus, knowledge of downhole pressure and temperature are needed. The third requirement is that formation injectivity be large enough for the CO_2 to be injected without large pressure increases, which would necessitate the drilling of multiple injectors, increasing costs, and could risk compromising the integrity of sealing layers. Good injectivity requires adequate permeability, which can be assessed by well logs, core analyses, and single-well and interference hydraulic tests. A more advanced capacity question is how efficiently CO_2 fills up the pore space within the storage formation. To answer this question requires a detailed knowledge of the physical and chemical behavior of the CO_2/brine system, which is also the information needed to ensure successful long-term trapping of the injected CO_2, as described in the next paragraph.

The requirements for long-term trapping of CO_2 in the subsurface have been described by several authors (e.g., van der Meer 1992, 1996; Bachu et al. 1994; Pruess et al. 2003) and are summarized here for geologic storage of CO_2 in saline formations. In the subsurface, CO_2 exists as an immiscible free phase, which is the non-wetting phase, and as a solute in the aqueous phase, which is the wetting phase. For typical hydrostatic pressure gradients and geothermal temperature gradients, CO_2 is supercritical at depths greater than about 800 m. Trapping CO_2 is a significant challenge because the low density of free-phase CO_2 compared to native brine (Fig. 1) makes it strongly buoyant, thus it will always try to move up toward the surface. Trapping CO_2 in the subsurface for long-term geologic storage can be accomplished by four primary mechanisms, the first three of which have been collectively referred to as hydrodynamic trapping by Bachu et al. (1994). (1) Stratigraphic or structural trapping: buoyant free-phase CO_2 is trapped beneath low-permeability layers or in faulted or anticlinal structures (Knox et al. 2003; Gunter et al. 2004; Ambrose et al. 2007). Knowledge of regional geology, geophysical imaging, and well logs provide this information. (2) Mobility trapping (also known as phase trapping, capillary trapping, residual trapping): multi-phase flow processes immobilize free-phase CO_2. Although free-phase CO_2 is actually supercritical, it is referred here to as the gas phase, in analogy with other two-phase systems (e.g., water/natural gas, water/steam) in which gas is the non-wetting phase. In the petroleum literature (e.g., Land 1968; Holtz 2002) it is commonly

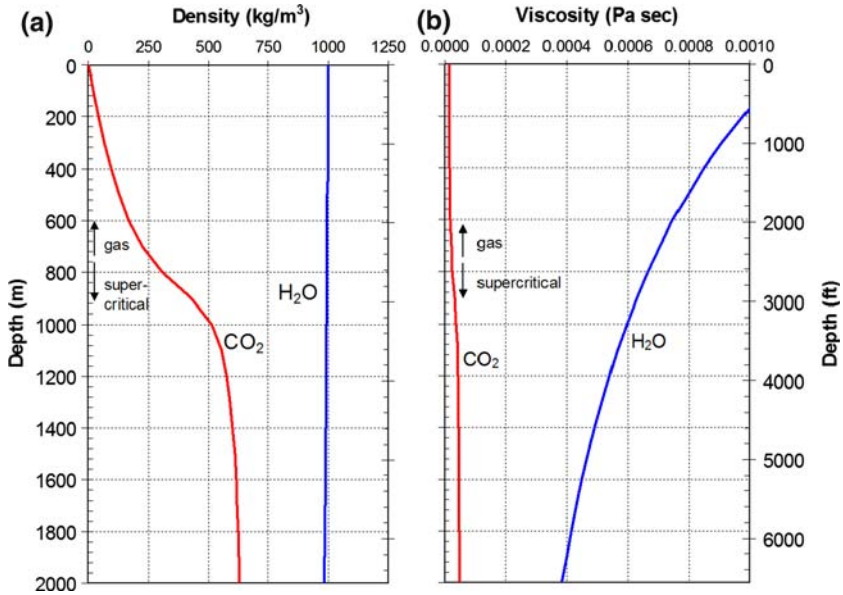

Fig. 1 Variation of **a** density and **b** viscosity with depth for CO_2 and water for surface conditions of 1 bar and 15°C, a hydrostatic pressure profile of 10 MPa/km, and a geothermal temperature gradient of 30°C/km, as calculated by the TOUGH2 simulator (Pruess et al. 1999; Pruess and García 2002)

assumed that residual gas saturation (the saturation below which CO_2 is immobile) is history-dependent, with a small value during the drainage process (CO_2 displacing brine), and a potentially large value during wetting (brine displacing CO_2), which increases as the maximum historical CO_2 saturation increases. This phenomenon can be modeled using hysteretic capillary pressure and relative permeability curves, as shown in Fig. 2. Measurements of the two-phase flow behavior of CO_2 and brine (Bachu and Bennion 2007) provide the best direct information for mobility trapping, but information from other two-phase flow systems also can be valuable. Laboratory experiments are very useful, but upscaling is far from trivial, so field experiments are even better. Several recent modeling studies of field-scale mobility trapping (Kumar et al. 2005; Mo and Akervoll 2005; Spiteri et al. 2005; Doughty and Myer 2007), investigate the sensitivity of mobility trapping to various hydrologic parameters, but none include a comparison to field data. (3) Dissolution trapping: the CO_2 that dissolves in brine is no longer buoyant so there is no driving force toward the surface. In fact, CO_2-saturated brine is denser than native brine. As CO_2-laden brine sinks deeper into the formation it can set up circulation patterns that enable more free-phase CO_2 to come into contact with native brine, enabling more dissolution to occur (Lindeberg and Wessel-Berg 1997; Ennis-King and Paterson 2005;

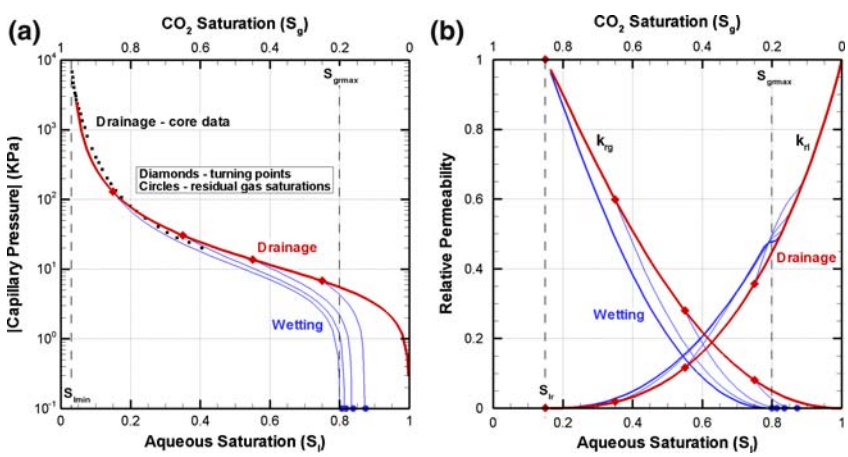

Fig. 2 Typical hysteretic characteristic curves used for modeling the Frio brine pilot: **a** absolute value of capillary pressure and **b** relative permeability. All grid blocks follow the *red curves* while they are undergoing drainage. The *diamonds* illustrate a few of the infinitely many possible turning points from drainage to wetting, which define the wetting curve for each grid block and the corresponding value of residual gas saturation S_{gr}^{Δ} (*circles*). *Black symbols* show capillary pressure data obtained from mercury-injection laboratory experiments on core samples from the injection well (Sakurai et al. 2005)

Riaz et al. 2006). Brine composition, which may be determined by collecting undisturbed fluid samples, is needed to quantify CO_2 dissolution. (4) Mineral trapping: CO_2 reacts with rock minerals to form carbonate compounds (Gunter et al. 1993; Pruess et al. 2003; Johnson et al. 2004). Mineral compositions and distributions, which may be obtained from core samples, are needed to quantify CO_2/mineral chemical reactions.

Because of the complexity and variety of processes occurring in CO_2/brine systems, development and application of a numerical model concurrently with site characterization is extremely valuable. Simulation results provide a detailed picture of CO_2 plume evolution in space and time, hence they can be helpful in interpreting field observations, which are typically sparse in space or time or both. Additionally, by comparing simulation results to field observations, one may infer values of poorly known parameters and incorporate new features in the conceptual and numerical model of the site. Finally, numerical modeling can be used to help design field tests and predict test outcomes to assess the validity of the conceptual model.

Case study: the Frio brine pilot

At the Frio brine pilot, a research project conducted at the South Liberty oil field operated by Texas American Resources in Dayton, Texas, USA (Fig. 3), 1,600 metric tons of CO_2 were injected over a period of 10 days into a steeply dipping brine-saturated sand layer at a depth of 1,500 m (Hovorka et al. 2006). At this depth, free-phase CO_2 is supercritical. The pilot employed one injection well and one observation well. Pre-injection activities included traditional site-characterization techniques such as review of the regional geological setting, development of a detailed local geological model, analysis of wireline logs, laboratory analysis of core samples, collection and chemical analysis of brine samples, pressure-transient analysis of an interference well test, and breakthrough curve analysis for a two-well recirculation tracer test. Additionally, the CO_2 injection itself served as a two-well tracer test and an interference well test. Geophysical monitoring of CO_2 movement in the subsurface during and after the injection period provided information on the spatial distribution of CO_2 at several different scales. Frio brine pilot activities are outlined in Table 1, and are described in the following sections. Table 2 summarizes the material properties and formation conditions inferred from traditional site characterization and Tables 3 and 4 present the findings from CO_2 injection and monitoring.

Numerical modeling has been an integral part of the Frio brine pilot from the outset. Initially, modeling helped design parameters of the pilot test such as well spacing, target sand thickness, and quantity of injected CO_2, as well as pre-injection well-test procedures (Doughty et al. 2003, 2004; Hovorka et al. 2004). Then, the model was used to predict the results of the pilot prior to its execution (Doughty et al. 2004; Holtz et al. 2004). Finally, simulation results were compared with observations from various monitoring techniques (Freifeld et al. 2005a; Trautz et al. 2005; Hovorka et al. 2006). This sequence of activities followed the standard approach of model development based on traditional site-characterization, followed by model application to predict CO_2 transport. In contrast, the sections that follow emphasize the role that modeling CO_2 injection plays in site characterization itself.

Traditional site-characterization activities

In the vicinity of the South Liberty field, the fluvial-deltaic Frio formation is overlain by the regionally extensive, low permeability Anahuac shale, which acts as a regional upper seal for the Frio formation sands. Individual sand layers, identified as A, B, C, etc., are separated by more localized shale layers that also serve as barriers to flow. At the South Liberty field, numerous wells drilled for historical oil production at depths around 2,400 m provide structural information about the site (Hovorka et al. 2006). The brine-saturated sand layer targeted for CO_2 storage, the C sand, is near the top of the Frio formation at a depth of 1,500 m and is on the flank of a salt dome (Fig. 4), where the Frio formation is laterally compartmentalized by faults (Fig. 5). A new injection well was drilled for the Frio brine pilot, sited 32-m down dip (south) from an existing well that served as the observation well. The fault block in which the wells lie is about 800 m across and at least 2,500 m long,

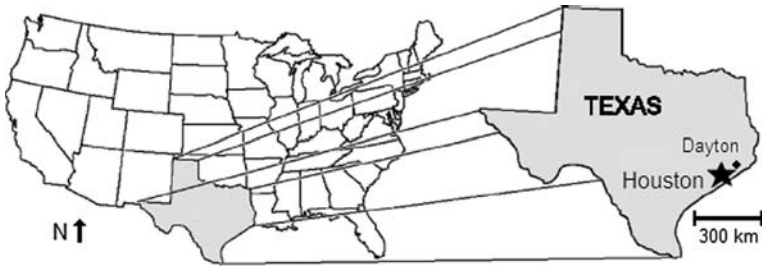

Fig. 3 Location map for the Frio brine pilot, conducted at the South Liberty field, near Dayton, Texas, USA, about 60 km northeast of Houston

Table 1 Activities at the Frio brine pilot

Activity	Monitoring	Information obtained
Review existing data related to historical oil production	3D seismic	Structure of sand and shale layers surrounding salt dome
	Wireline logs in regionally distributed wells	Compartmentalization into fault blocks
Well log analysis	Wireline logs in injection and observation wells	Target sand layer and overlying shale cap rock
		Extent, continuity, and variability of layers
		Permeability, porosity, relative permeability parameters (estimated using literature correlations)
Core analysis from newly drilled injection well	Porosity	Calibration for well-log estimates of porosity and permeability
	Permeability	
	Mercury injection	Capillary pressure/saturation relationship
Interference well test	Pressure transients	Inter-well connectivity
		Flow properties of lateral boundaries
		Field-scale permeability
		Estimates of pressure increase during CO_2 injection
Aqueous-phase tracer test	Fluorescein breakthrough curve (BTC)	Single-phase dispersivity
		Porosity-thickness product of sand layer
		Sorption
CO_2 injection and post-injection rest period	CO_2 arrival at observation well	Average CO_2 saturation between wells
	Pressure transients	Two-phase flow properties
	RST (reservoir saturation tool)	CO_2 saturation profiles at injection and observation wells
	Crosswell seismic	CO_2 distribution between injection and observation wells
	VSP (vertical seismic profile)	CO_2 distribution updip of observation well
Two-phase tracer test (concurrent with CO_2 injection)	Two-phase tracer BTC	Two-phase dispersivity
		Evolution of CO_2 saturation distribution with time

and is bounded by mapped faults to the northwest and southeast. Several smaller intra-block faults also exist, with offsets that may juxtapose the B and C sands, enabling fluid flow between them.

Figure 6 shows the porosity and horizontal permeability profiles for the C sand inferred from injection-well logs, with calibration to porosity and permeability measurements made on core samples (Sakurai et al. 2005). Observation-well logs (not shown) contain similar features, suggesting good layer continuity between the two wells. The ratio of vertical to horizontal permeability is determined as an increasing function of porosity, based on correlations of Holtz (personal communication, 2002), and ranges from 0.1 for porosity <0.24 to 1.0 for porosity >0.28. Each well was perforated over approximately 6 m in the upper portion of the 23-m thick C sand, which Fig. 6 identifies as a thick interval of clean sand. The lower limit of the injection interval is delineated by a thin marker bed, which is interpreted as low-permeability shale. Capillary pressure as a function of saturation was measured for two core samples, one sandstone and one shale, using mercury injection (Sakurai et al. 2005); results for the sandstone are shown in Fig. 2a.

Frio formation brine samples were collected from both wells at a series of times before CO_2 injection. Chemical analysis identified a Na–Ca–Cl-type brine with 93,000 mg/L total dissolved solids (TDS), nearly saturated with methane (CH_4) at formation conditions of about 150 bars and 60°C (Kharaka et al. 2006). These dissolved salt and methane contents are typical of brine formations found in the vicinity of petroleum resources in the northern Gulf of Mexico basin (Kharaka and Hanor 2004).

The three-dimensional (3D) numerical model developed for the Frio brine pilot represents the C sand and extends over the entire fault block in which the injection and observation well lie, and is an idealized version of the geological model shown in Fig. 5. A schematic diagram of the numerical grid is shown in Fig. 7. The model is 23 m thick, with closed upper and lower boundaries to represent continuous shale layers over and underlying the C sand. Instead of the geological model's warped layers that curve

Table 2 Material properties and formation conditions obtained from traditional site-characterization

Property	Method	Value	Comments
Injection interval (thickness of high-permeability clean sand), h	Wireline logs	5.5 m	Figure 6b
	Match tracer test BTC	8 m (assuming no sorption)	Figure 9
		5.5 m (assuming sorption)	Sorption and thickness varied, porosity held fixed at 0.34
Porosity, ϕ	Wireline logs calibrated to core analysis	0.34 average over 5.5-m injection interval	Figure 6a
		0.28 average over 23-m thick C sand	
Permeability, k	Wireline logs calibrated to core analysis	2,264 md average over 5.5-m injection interval	Figure 6b
		1,001 md average over 23-m thick C sand	
	Interference well test	Around wells: kh product consistent with wireline logs, low vertical permeability below clean sand creates leaky aquifer	Figure 8
		Far from wells: possibility of larger kh or constant-P boundary	For h = 5.5 m, average k ~ 2,300 md For h = 8 m, average k ~ 1,600 md near wells, ~3,100 md farther away
Hydrologic properties of small fault	Interference well test	No hydrologic effect	Figure 8
Formation compressibility, C	Interference well test	For h = 5.5 m, 1.88×10^{-9} Pa^{-1}	Figure 8
		For h = 8 m, 1.28×10^{-9} Pa^{-1}	Defined as $C = (1/\phi)\partial\phi/\partial P\|_T$
Capillary pressure parameters	Mercury injection on core samples	van Genuchten (1980) parameters: P_{c0} = 6,500 Pa, n = 1.7, S_{lmin} = 0.03 for a sample with k = 837 md	Figure 2a Curve-fit to drainage curves, also used for wetting curves $P_{c0} \sim k^{-1/2}$
Dispersivity, α	Match tracer-test BTC	0.1 m	Figure 9
Pressure, P	Downhole sensor	152 bars	
Temperature, T	Wireline logs, fluid sampling	59°C	Average of 56–65°C range obtained for different measurements
Salinity	Fluid sampling	0.093 mg/L	

in two directions, the model is a plane that is tilted upward 16° from south to north, to represent the local dip between the injection and observation wells. The lateral boundaries to the northwest and southeast are closed to represent impermeable faults bounding the block, the lateral boundary to the northeast is also closed to represent the termination of the C sand against the salt dome, and to the southwest, where no fault has been mapped, the model extends for a great distance beyond what is shown in Fig. 7a. The intersection of the small intra-block fault nearest the wells (Fig. 5) and the C sand is included in the model, located 88 m northwest of the observation well. Because offsets along this fault may provide connections between different sand layers within the upper Frio Formation, flow conditions at the fault/C-sand intersection are unknown, and several different possibilities are modeled. Vertical grid spacing varies to capture the key geological changes in porosity and permeability, as shown in Fig. 6, and lateral grid spacing is also variable (Fig. 7), with finer resolution around injection and observation well locations. In total, the model contains 22 layers, each composed of 40 by 36 grid blocks. The wells are represented as source or sink terms within 2-m by 2-m wide grid blocks, so model results for those grid blocks are representative of the

Table 3 Boundary conditions inferred from pressure transients obtained during CO_2 injection

Boundary	Fluid flow boundary condition
NW and SE block-bounding faults	Closed
NE salt dome	Constant pressure

Table 4 Comparison of model results to field data for various sets of multi-phase flow parameters

Multi-phase flow parameters*			Monitoring method				
S_{lr}	m	S_{grmax}	U-tube CO_2 arrival time at observation well 2.12 days (Fig. 11)	Pressure transients ΔP at observation well during CO_2 injection (Fig. 12)	RST S_g profiles in injection and observation wells during and after CO_2 injection (Fig. 13)	Crosswell seismic S_g distribution in plane between wells after CO_2 injection (Fig. 14)	VSP Azimuthal S_g profiles beyond wells after CO_2 injection (Fig. 15)
0.00	0.9	~0.2	2.7	Model ΔP a bit too big	Model S_g higher than base case, still too low	Same as base case	Same as base case
0.15	**0.9**	**~0.2**	2.3	Model ΔP a bit too big	Model S_g all too low	Good match	Good match updip, not enough lateral spreading
0.30	0.9	~0.2	1.9	Good match	Model S_g lower than base case	Same as base case	Same as base case
0.45	0.9	~0.2	1.5	Model ΔP a bit too small	Model S_g even lower	Same as base case	Same as base case
0.15	0.7	~0.2	1.6	Good match	Model S_g lower than base case	Same as base case	Same as base case
0.15	0.5	~0.2	1.1	Model ΔP too small	Model S_g even lower	Same as base case	Same as base case
0.15	0.9	~0.1	2.3	Same as base case	Model S_g too low	CO_2 plume moves a bit too much	CO_2 plume moves a bit too much
0.15	0.9	0	2.3	Same as base case	Model S_g far too low	CO_2 plume moves far too much	CO_2 plume moves far too much
5.5-m sand model							
0.15	0.9	~0.2	1.8	Same as base case	CO_2 not deep enough at injection well	Pretty good match, but CO_2 plume a bit too thin	Same as base case

Unless otherwise noted, simulations use the 8-m sand model

* The second set of parameters (in bold) define the base case

formation in the immediate vicinity of the well rather than conditions within the well itself.

Interference test

A 24-h interference well test was conducted by pumping from the observation well and observing pressure changes in both wells. Pumping rate was constant for the first 8 h, then gradually increased. Due to complications such as well-bore storage, skin effects, and local degassing of methane, the pressure transient at the observation well (the pumped well) is not analyzed. Figure 8 shows the pressure transient at the injection well (the non-pumped well) and several modeled pressure transients obtained with different analysis methods. The simplest method is to match the pressure transient to an analytical solution (Theis 1935), which assumes a uniformly thick, homogeneous, flat layer of infinite radial extent that is perfectly sealed above and below, and a constant pumping rate. A good match to the early-time portion of the pressure-transient data can be obtained with the Theis solution (curve labeled "Theis" in Fig. 8), using a layer thickness of 5.5 m, a porosity of 0.34 and a permeability of 2,264 md (depth-averaged values for the 5.5-m thick perforated interval in the injection well, see Fig. 6), and a formation compressibility of 2.2×10^{-9} Pa^{-1}. The Theis curve begins to deviate from the field data after about one-half hour of pumping, predicting too large a pressure drawdown. A one-layer radially symmetric numerical model with the same formation properties as the Theis solution, but with a variable pumping rate, produces a comparably good match at early times (not shown). The upturn in pressure drawdown in response to the increase in pumping rate at 8 h is reproduced, but the absolute value of pressure drawdown is too large for all times after one-half hour.

Next, the interference test is simulated with the 3D model shown in Fig.7. Assigning a very low permeability for the marker bed below the perforated interval effectively constrains the hydrologic response to the upper 5.5 m of the C sand, and produces a pressure drawdown comparable to the Theis solution (not shown). With the actual marker bed permeability inferred from Fig. 6b (30 md horizontal permeability, 3 md vertical permeability), the pressure drawdown obtained with the 3D model becomes too small after only about 10 s (curve labeled "Original Model" in Fig. 8). A nearly identical pressure drawdown (not shown) is obtained using a high-resolution multi-layer radially symmetric (RZ) model that has 153

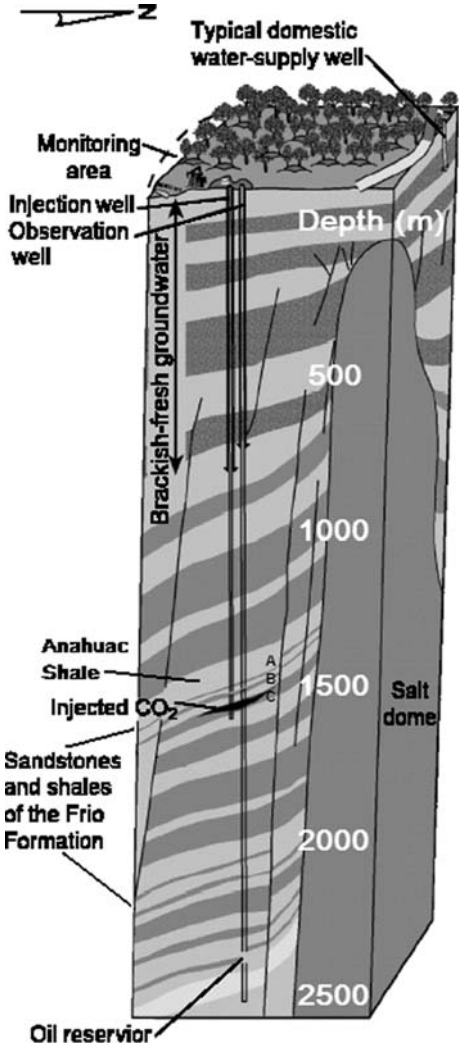

Fig. 4 Schematic of the Frio brine pilot site (after Hovorka et al. 2006). *Dark layers* show sandstones and *light layers* indicate shales. CO_2 injection depth is about 1,500 m and historical oil production depth was about 2,400 m

layers, each 0.5 ft (0.152 m) thick, which is the resolution at which the injection-well wireline logs were sampled. This vertical resolution enables porosity and permeability values obtained from the logs of the C sand (Fig. 6) to be assigned to the model directly, with no need for vertical averaging. The similarity of the results of the high-resolution RZ model and the 3D model indicates that the averaging procedure shown in Fig. 6 does not introduce significant errors. Additionally, the RZ model extends far enough radially to be infinite acting, and small late-time deviations between the RZ and 3D models indicate that the closed lateral boundaries of the 3D model are not felt until 8 h after pumping begins. Hence the large discrepancy between the original model pressure drawdown after 10 s and the field data is not due to numerical limitations of the 3D model.

Figure 8 shows that the field data do not have the linear character of the Theis solution or the original model pressure drawdown between 0.5 and 8 h, but rather show a marked flattening. Such a response is characteristic of a constant-pressure boundary or large increase in permeability some distance from the wells. It is also the hallmark of a leaky aquifer, in which fluid flows to the pumped well from both the pumped interval and to a lesser extent from above and/or below (Hantush and Jaocb 1955). Note from Fig. 6b that the permeability just above the pumped interval is very low, but that the permeability of the marker bed below the pumped interval is moderate. By decreasing the vertical permeability of the marker bed from 3 to 0.25 md, the pressure drawdown labeled "leaky 5.5-m sand, no small fault" in Fig. 8 is obtained, in which the observed flattening beginning at 0.5 h is much better represented. This parameter change is not considered unreasonable (i.e., it is within the uncertainty typical of well-log analysis), so it is retained for further modeling studies.

To investigate the hydrologic nature of the intersection of the small fault northwest of the observation well and the C sand, three distinct fault conditions are considered with the 3D model: (1) the fault is absent (curve labeled "no small fault" in Fig. 8), (2) the fault is a closed boundary (curve labeled "closed small fault" in Fig. 8), and (3) the fault is a constant-pressure boundary (curved labeled "open small fault" in Fig. 8). The effect of the small fault is felt about 0.5 h after pumping begins. Both the closed-fault case and the constant-pressure-fault case diverge sharply from the field data, suggesting that the fault does not act as either of these types of boundaries, and in fact produces no distinctive hydrologic response.

Figure 8 shows that after about 4 h of pumping, the observed pressure drawdown flattens more than the leaky-aquifer model can account for, suggesting that some distance from the wells, formation permeability increases, the clean sand thickens, or a constant-pressure boundary is present. Higher temperature (smaller viscosity) or the presence of a gas cap (larger compressibility) could also contribute to the flattening. The well test was simulated with several modified 3D models that included different combinations of these features, producing good matches to the late-time observed pressure-drawdown data (not shown). Despite the satisfaction of obtaining much-improved matches to the field data, the model changes made to achieve them are not uniquely determined. Furthermore, because of the possibility that the late-time flattening is caused by an effect specific to pressure decrease (e.g. methane degassing creating a high-compressibility two-phase region), these features are not retained for the modeling of the CO_2 injection, when pressures increase.

As will be presented in the next section, there is independent evidence from the tracer test that the thickness of

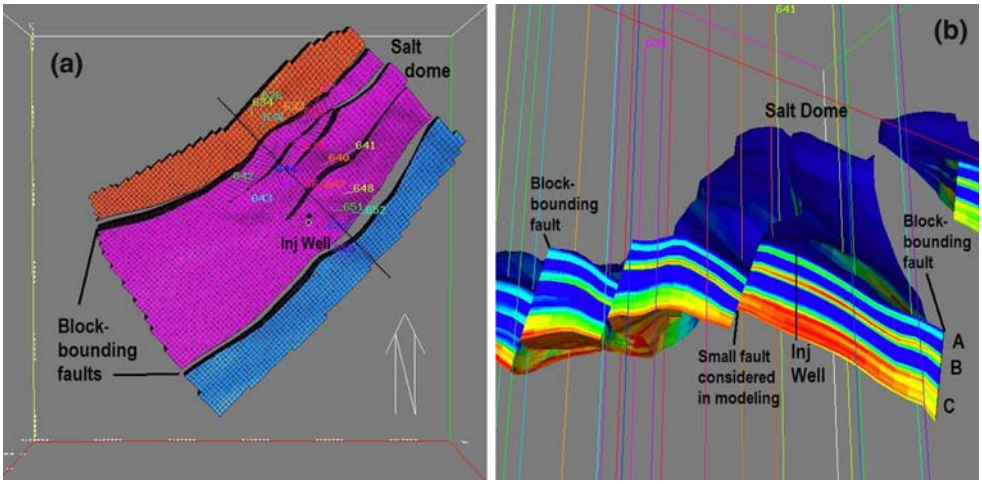

Fig. 5 Geological model of the upper Frio formation at the South Liberty field (courtesy of Joseph Yeh, TBEG). **a** Plan view of the modeled fault block (*pink*) and two adjacent fault blocks (*red* and *blue*). The new injection well is shown as a *black dot* with a *white border*. The existing observation well is the *black dot* just to the north. **b** Vertical cut through the model along the *black line* shown in the plan view. Vertical exaggeration is approximately a factor of two. Coloring shows a stochastic porosity distribution (not used in numerical model). *Colored lines* and numbers identify wells used to create the geological model

the high-permeability clean sand in which the injection well is perforated is about 8 m, significantly larger than the 5.5 m inferred from the well logs. Because the pressure drawdown response to pumping is primarily sensitive to the permeability-thickness product of a formation, it is worthwhile to investigate how well the interference test can be modeled assuming an 8-m thick layer of clean sand. It turns out that a pressure drawdown nearly indistinguishable from the "leaky 5.5-m sand, no small fault" curve of Fig. 8 can be obtained by (1) increasing the permeability for the three model layers just below the injection well perforated interval to 2,000 md (effectively making the high-permeability clean sand 8 m thick), (2) reducing all permeability and formation compressibility values within 200 m of the wells by a factor of 5.5/8 relative to the 5.5-m model, (3) assigning the vertical permeability of the layer below the clean sand, which controls leakage, a value of 0.5 md, and (4) increasing the far-field permeabilities (>200 m from the wells) by a factor of 1.36 relative to the 5.5-m model. Together, changes (1) and (2) preserve the permeability-thickness product of the clean sand. Changes (3) and (4) were made by trial and error to improve the model's match to the observed pressure-drawdown data. All of these changes are considered reasonable, considering the spatial variability expected for the fluvial-deltaic geologic setting. The modified model is referred to as the "8-m sand model"

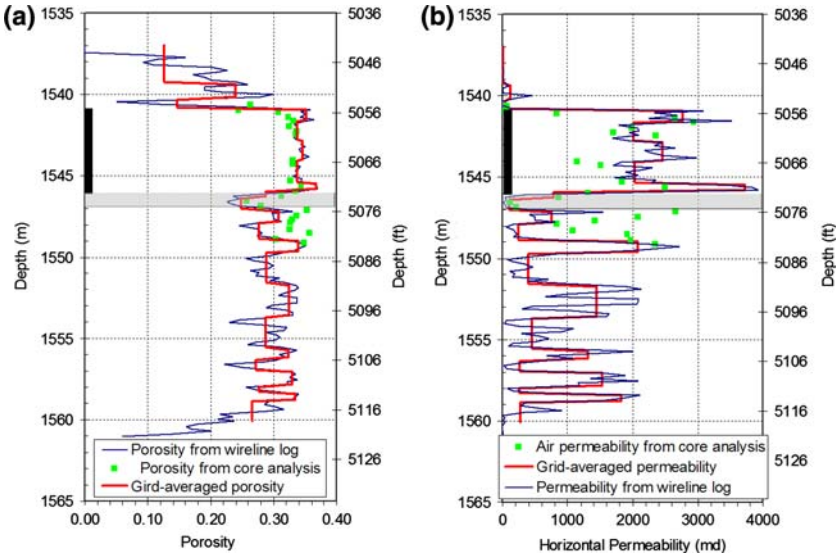

Fig. 6 Injection-well property profiles for the C sand (courtesy of Shinichi Sakurai, TBEG), and the grid-averaged values used for the original 3D numerical model: **a** porosity and **b** horizontal permeability. The injection-well perforated interval is shown as a *black bar* and a low-permeability marker bed that delineates the bottom of the injection interval is shown with *gray* shading

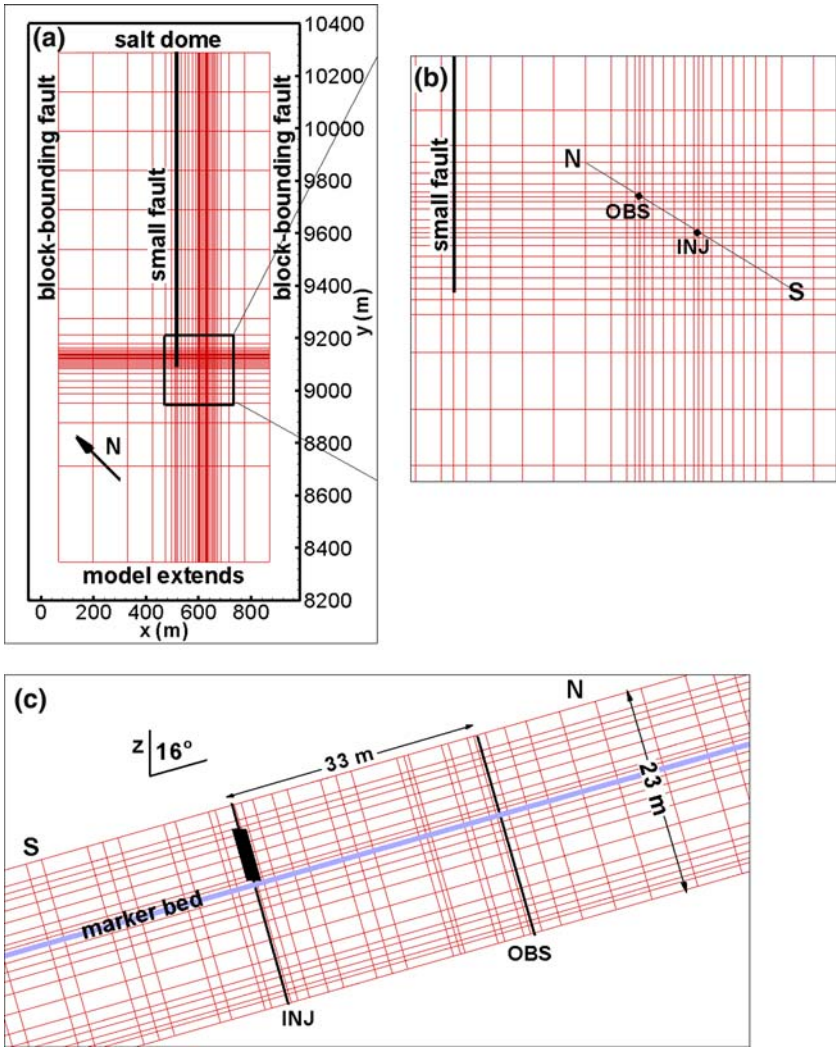

Fig. 7 3D model grid: **a** plan view; **b** plan view of local area around wells; **c** vertical cross-section between injection and observation wells. The injection-well perforated interval is shown as a *black bar*

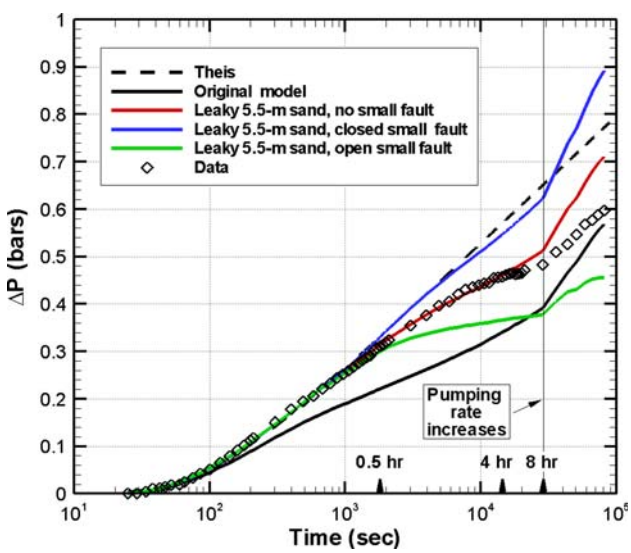

Fig. 8 Interference-well-test pressure transient for injection well (the non-pumped well) and various model results

and the original model with marker-bed vertical permeability reduced to 0.25 md is referred to as the "5.5-m sand model".

In summary (Table 2), matching the injection-well (non-pumped well) pressure transient during the interference well test does not provide a single, uniquely-determined hydrologic model of the C sand, but rather two models that bound a range of reasonable models. Assuming that the high-permeability clean sand over which the injection well is perforated has a thickness of 5.5 m, the average permeability of the C sand within a few hundred meters of the wells is generally consistent with values obtained from core samples and wireline logs (~2,300 md). If the thickness of the clean sand is increased from 5.5 to 8 m, the average permeability near the wells correspondingly decreases from about 2,300 to 1,600 md. In either case, the clean sand acts as a leaky aquifer. Sensitivity-study results indicate that the small fault within the main fault block should not be considered either a closed or

constant-pressure boundary, therefore it is not included in further modeling studies. It appears that farther from the wells, either the sand thickens or constant-pressure conditions may exist. This finding is not expected to impact the movement of the small amount of CO_2 used for the pilot test, but could be critical for full-scale CO_2 storage.

Tracer test

After the interference well test had run for 24 h, pumped fluid was reinjected into the injection well, to create a balanced doublet flow field. After another 24 h, when the flow field was steady, a 78-min pulse of fluorescein dye was added at the injection well. The steady flows were maintained for 15 days. Fluorescein arrived at the observation well after 9 days and concentration peaked at 12 days, as shown in Fig. 9**.** The primary parameters to be inferred from the tracer breakthrough curve (BTC) are the porosity-thickness product of the sand layer through which fluid flows and the aqueous-phase dispersion coefficient for the sand, a measure of its heterogeneity. Preliminary attempts to model the tracer test using the 3D model described in the previous section were unsatisfactory, because numerical dispersion smeared out the tracer peak too much for a physical dispersion coefficient to be determined. Therefore, a streamline model (Javandel et al. 1984) is used, with a random walk added to represent dispersion. Figure 9 presents modeled breakthrough curves for two different sand-layer thicknesses: the 5.5-m value inferred from the injection well logs (Fig. 6), which results in a far too early peak, and an 8-m value, determined by trial and error to best match the observed fluorescein peak time of 12 days. In both cases, porosity is held fixed at 0.34, the average value obtained from wireline logs and core analysis. Note that the model breakthrough curves show two

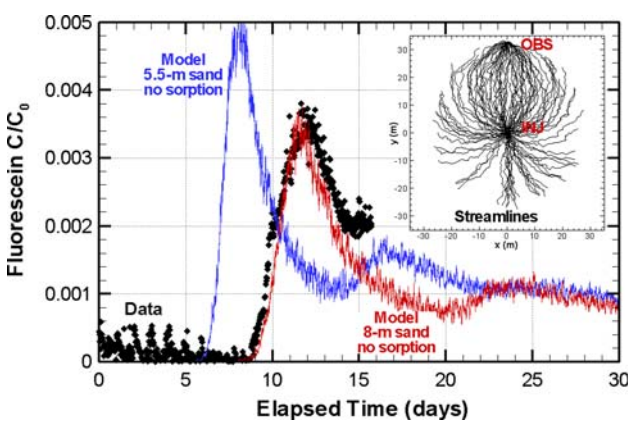

Fig. 9 Tracer test data and results of a streamline model. For each model, porosity is 0.34 and dispersivity is 0.1 m. Model results show a main peak (8 or 12 days) and a smaller recirculation peak (16 or 24 days)

peaks, the main peak and a smaller, later recirculation peak, which identifies tracer that has arrived at the observation well, been reinjected into the injection well, and traveled to the observation well again. Matching the width and height of the observed fluorescein peak requires a small single-phase dispersivity (0.1 m), implying that the sand is highly homogeneous, which is considered reasonable for a clean sand. Essentially equivalent results for dispersivity and thickness were obtained by Trautz et al. (2005) using the analytical approach of Grove and Beetem (1971).

The 8-m sand thickness inferred from tracer arrival time is certainly possible in terms of the expected variability in sand layer thickness for this geologic setting, and, as described in the previous section, interference test results can be equally well matched assuming either a thickness of 5.5 or 8 m for the high-permeability zone in which the injection well is perforated. However, another possibility is that the fluorescein transport is being retarded by sorption. Fluorescein is generally considered to be a relatively conservative tracer in groundwater and geothermal systems, but studies reported in the soils literature (where organic content of soils is high) indicate that fluorescein does sorb to organics (Smart and Laidlaw 1977). It may be that the high concentration of dissolved methane present in the Frio Formation brine promotes sorption. Under the assumptions of the streamline model, tracer travel time depends only on the product of formation thickness, porosity, and a retardation factor that equals one for non-sorbing tracers and is greater than one for sorbing tracers (Javandel et al. 1984). Thus, a model with a sand thickness of 5.5 m and a retardation factor of 8/5.5 and a model with a sand thickness of 8 m and a retardation factor of one (no sorption) would yield identical breakthrough curves for the main peak. The recirculation peaks for the two cases would differ because no (or at least far less) sorption occurs the second time the tracer moves through the formation. Hence one signature of a sorbing tracer would be a recirculation peak with a travel time of less than twice the travel time of the main peak.

In the field, it does not appear that tracer monitoring continued long enough for a recirculation peak to arrive: the 8-m no-sorption model predicts a recirculation peak at 24 days (Fig. 9), and a 5.5-m with-sorption model would predict a recirculation peak at about 20 days (12 days for the main peak to arrive plus at least an 8-day travel-time for a less-sorbing second trip through the formation). The increase in fluorescein concentration observed at 15 days (Fig. 9) is considered unlikely to be a recirculation peak, as it would imply a 3-day less-sorbing second trip through the formation, which in turn would imply a sand thickness of about 2 m and a retardation factor of about four, neither of which is consistent with other data from the field. Thus,

neither an 8-m thick, non-sorbing sand layer nor a 5.5-m thick, sorbing sand layer can definitely be eliminated from consideration. Therefore, both the 8-m sand model and the 5.5-m sand model described in the interference-test section are retained for further modeling studies.

CO_2 injection and monitoring

Numerical model for multi-phase flow

The well-test and tracer-test described above involve single-phase flow in which gravity does not play a significant role, enabling analysis with an analytical solution or simple numerical models. However, when CO_2 and brine are both present, multi-phase and gravity effects are significant, requiring a 3D numerical model with two-phase flow capabilities. TOUGH2 (Pruess et al. 1999) is a general-purpose numerical simulator for multi-phase, multi-component fluid and heat flow in porous and fractured media. It uses a multi-phase extension of Darcy's law that includes relative permeability and capillary-pressure effects and incorporates accurate phase-partitioning and thermophysical properties of all fluid phases and components. The present studies utilize a hysteretic formulation for capillary pressure and relative permeability (Doughty 2007) and an equation of state package called ECO2 (Pruess and García 2002), designed to treat a two-phase (liquid, gas), three-component (water, salt, CO_2) system in pressure/temperature regimes above the critical point of CO_2 (P = 73.8 bars, T = 31°C). Note that methane is not included in ECO2, but that the C-sand brine composition indicates near-saturated conditions for dissolved methane. Because the presence of methane decreases the solubility of CO_2, the present model would be expected to overestimate the amount of CO_2 that can dissolve in the brine. Preliminary simulations using EOS7C (Oldenburg et al. 2004), a TOUGH2 equation of state package that includes CH_4 and CO_2 (but no salinity effects), suggest that the effect is minor because CH_4 is largely purged from the formation where the CO_2 plume develops. Although TOUGH2 has the capability to solve fully coupled fluid and heat flow problems, temperature is assumed to remain constant for the present simulations, to increase computational efficiency. A few simulations were repeated without this assumption, but the results did not differ significantly from those presented here.

The numerical simulations for the Frio brine pilot discussed here are all of short duration (lasting no more than a few months), hence they emphasize advective processes. Slower flow processes such as aqueous-phase diffusion of dissolved species and the buoyancy effect of dissolved CO_2 are not included in the numerical model. Salt may precipitate out of the brine, but the rock matrix itself is inert. Thus, chemical reactions between CO_2 and rock minerals that were inferred from geochemical analysis of brine samples collected during the CO_2 injection period (Kharaka et al. 2006) are not considered.

Together, capillary pressure P_c, liquid relative permeability k_{rl}, and gas relative permeability k_{rg} are known as characteristic curves; they control the way the brine (the wetting phase, also called the liquid phase) and supercritical CO_2 (the non-wetting phase, also called the gas phase) interact. In a hysteretic formulation, P_c, k_{rl}, and k_{rg} depend not only on the saturation of the grid block, but also on the history of the saturation of the grid block. When liquid saturation decreases because more CO_2 enters a grid block than leaves it, the process is known as drainage. Alternatively, when liquid saturation increases because more brine enters a grid block than leaves it, the process is known as imbibition or wetting. Some parameters within the characteristic curve functions depend only on what process is occurring, so it is convenient to subdivide the characteristic curves into drainage branches and wetting branches (Fig. 2). Other parameters depend on the value of the saturation when the grid block makes a transition from drainage to imbibition or vice versa, the so-called turning-point saturations (Fig. 2). Because turning-point saturations differ among all grid blocks, these parameters do as well. The most critical parameter is the residual gas saturation, denoted S_{gr}^{Δ}, which is the saturation below which gas is immobile (i.e., the saturation below which immiscible CO_2 is trapped). In the petroleum literature (e.g., Land 1968; Holtz 2002) it is commonly assumed that under drainage conditions, $S_{gr}^{\Delta} = 0$, but for imbibition, S_{gr}^{Δ} increases as the turning-point saturation between the drainage curve and wetting curve, denoted S_l^{Δ}, decreases, as shown in Fig. 2. Thus, grid blocks that once contained the most CO_2 are those which trap the most CO_2. The maximum possible value of S_{gr}^{Δ} is S_{grmax}, which is obtained for the minimum possible value of S_l^{Δ}, which is generally equal to the irreducible liquid saturation S_{lr}.

The simulation results shown here use the capillary pressure curve shown in Fig. 2a, obtained by fitting to mercury injection data from a C-sand core sample (Sakurai et al. 2005), and the relative permeability curves shown in Fig. 2b. The key parameters of the characteristic curves that need to be identified are the maximum residual gas saturation S_{grmax} and irreducible liquid saturation S_{lr}, below which each phase is immobile, and a parameter describing the interference between the two phases when both are mobile. For the present hysteretic relative permeability functional forms (Doughty 2007), which are derived from the van Genuchten (1980) formulation, this interference is quantified by a parameter known as m, which can range from about 0.4 to 0.9, with lower values of m corresponding to more mobile gas and less mobile liquid, and higher values of m corresponding to less mobile gas and

more mobile liquid. During a CO_2 injection period, drainage is the dominant process because the CO_2 plume is growing in all directions. Hence, $S_{gr}^{\Delta} = 0$, and the parameters controlling plume behavior are S_{lr} and m. After injection ends, the leading edge of the CO_2 plume may still undergo drainage as the plume moves upward and updip by buoyancy forces, but at the trailing edge of the plume imbibition occurs, with S_{grmax} controlling trapping through S_{gr}^{Δ}.

Previously, simulations of the Frio brine pilot used values of S_{grmax} and S_{lr} taken from the literature: S_{grmax} varies inversely with porosity and averages 0.2 for the C sand (M. Holtz, personal communication, 2002; Holtz, 2005); S_{lr} = 0.3 (Pruess et al. 2003). The parameter m was chosen to produce a liquid relative permeability curve similar to a Corey (1954) liquid relative permeability curve (m = 0.9). In the present study, simulations were also run with values of S_{grmax} that are half the literature values and taking S_{grmax} = 0 for all materials, with S_{lr} values of 0, 0.15, and 0.45, and with m values of 0.7 and 0.5. The parameter set consisting of the original values of S_{grmax} (~0.2), S_{lr} = 0.15, and m = 0.9 form the base case against which other simulation results are compared. Comparison with recent laboratory experiments on CO_2/brine flow through sandstone cores (Bachu and Bennion 2007; L. Miljkovic, personal communication, 2006) indicates that the base-case parameters are reasonable for high-permeability sandstone.

Figure 10a shows a time-series of snapshots of the modeled free-phase CO_2 plume using the base-case parameters and the properties shown in Table 2, for the 8-m sand model. It is clear that buoyancy forces have a large effect on plume evolution, so much so that the 5.5-m sand model produces similar CO_2 distributions (Fig. 10b). The primary difference between the CO_2 distributions from the 8-m sand model and those from the 5.5-m sand model is a slightly stronger buoyancy flow for the 5.5-m sand model, which occurs because the permeability is slightly larger, and results in an earlier arrival of CO_2 at the observation well. Figure 10 also shows that CO_2 distributions for times later than 29 days are very similar to one another, indicating that by that time most gas saturations have decreased to residual values and the CO_2 plume is largely trapped.

U-tube

Sampling of representative fluids in deep boreholes is challenging because of the need to minimize external contamination and maintain sample integrity during recovery. The U-tube sampling methodology (Freifeld et al. 2005b; Freifeld and Trautz 2006) was developed to collect large volume, multi-phase samples at in situ pressures. At the Frio brine pilot, a U-tube was used to collect a 52-L sample from the observation well every 2 h, which was weighed at the surface while being maintained at downhole pressure conditions (~150 bars). A decrease in sample density from that of formation brine (~1,070 kg/m^3) to that of supercritical CO_2 (~830 kg/m^3) revealed the transition from single-phase brine to single-phase CO_2 in the wellbore 2.1 days after injection began (Fig. 11).

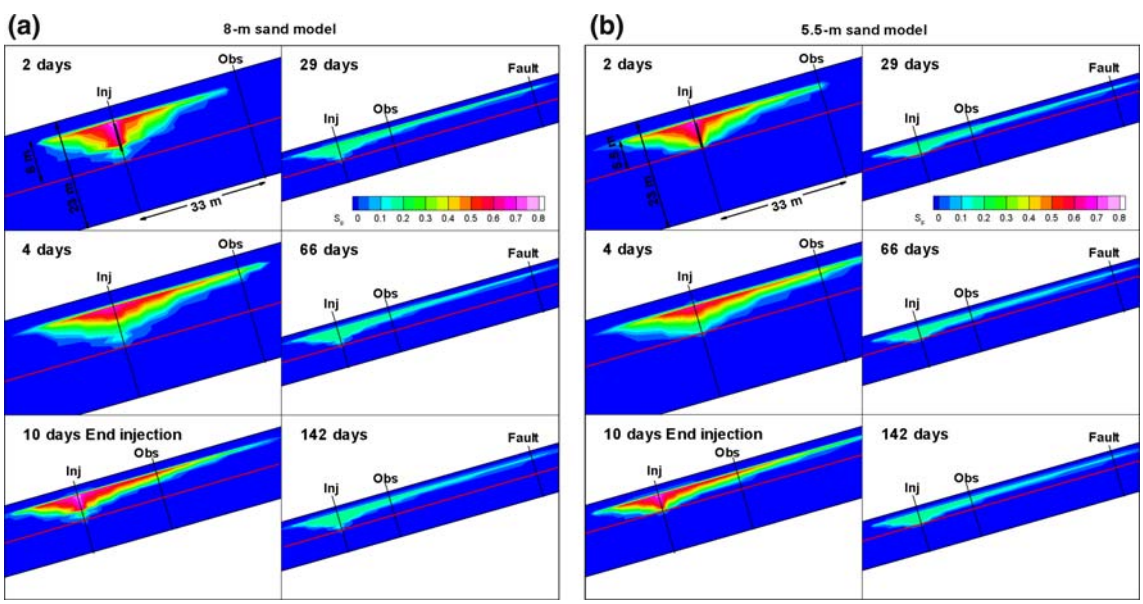

Fig. 10 Base-case simulation results showing the evolution of the free-phase CO_2 plume in the vertical cross-section containing the two wells. The *red line* shows the location of the low-vertical-permeability layer that bounds the high-permeability sand above it. **a** 8-m sand model; **b** 5.5-m sand model

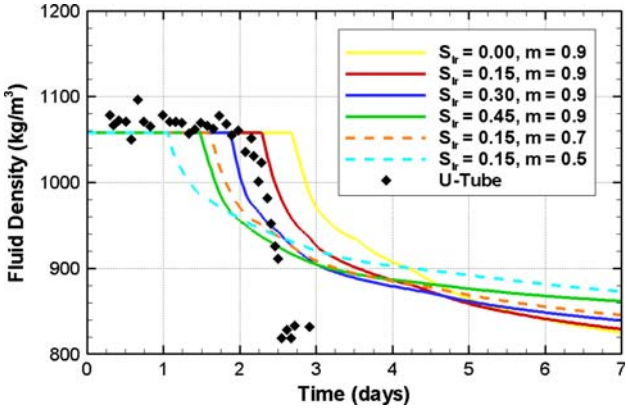

Fig. 11 CO_2 arrival at observation well as monitored with U-tube sampling and model results for the 8-m sand model considering different two-phase flow parameters

Analysis of sample gases (dissolved or separate phase) was performed in the field using a quadrupole mass spectrometer, which also provided unequivocal evidence of the arrival of the CO_2 plume. Additionally, pulses of gas-phase tracers were added to the injection stream at several times during the CO_2 injection period, and their arrival at the observation well provided an indication of changes in CO_2 saturation as injection proceeded.

During the 10-day injection period the CO_2 plume is continually growing, so the formation is undergoing drainage. Therefore, fluid flow (and hence observation-well arrival time) is sensitive to S_{lr} and m, but is not sensitive to S_{grmax}. The CO_2 injection period was modeled with the 8-m sand model using several values of S_{lr} and m, as shown in Fig. 11. Note that the U-tube sample density decreases much more than any of the model densities do. Recall that model density represents fluid density in the near-well region, not the density of the wellbore fluid itself, which is what the U-tube samples. Although the formation fluid is a two-phase mixture of CO_2 and brine, as the fraction of CO_2 increases, the mobility of the CO_2 becomes much greater than that of the brine (Fig. 2b), and far more CO_2 than brine flows into the wellbore. Therefore, when comparing model and field results, the time of the initial density decrease is used to indicate the CO_2 arrival, whereas the final value of density is assumed to reflect the relative mobility of the brine and CO_2 phases flowing into the wellbore rather than the formation saturation.

Figure 11 shows that models using S_{lr} = 0.15 or 0.30 and m = 0.9 give the best match to the field data, and that CO_2 arrival time decreases as S_{lr} increases and as m decreases. Larger values of S_{lr} cause a decrease in CO_2 arrival time two ways. First, with a larger S_{lr}, CO_2 bypasses more immobile brine, so it moves faster through the formation. Second, increasing S_{lr} increases total mobility (the sum of liquid- and gas-phase mobilities), hence it enables more buoyancy flow to occur, resulting in an early arrival of a thin finger of CO_2 shallow in the observation well (a more extreme version of what is seen in Fig. 10a). Decreasing m also increases total mobility and therefore enhances buoyancy flow. Likewise, the early arrival of CO_2 obtained with the 5.5-m sand model (not shown) arises not because of the smaller thickness of the sand, but because of its greater permeability, which allows more buoyancy flow.

It is worthwhile to note that the travel time between the two wells is much longer for the aqueous-phase fluorescein tracer (~9 days, Fig. 9) than for the two-phase CO_2 plume (~2 days, Fig. 11). Various factors contributing to this difference are presented in Table 5. Differences in the flow fields imposed by injection and pumping conditions (doublet for the tracer test, single-well for the CO_2 injection, lower injection rate for CO_2) tend to delay the CO_2 arrival, but the delay is more than balanced by the speedup arising from the buoyant, two-phase nature of the CO_2 plume. The modeled distribution of CO_2 (Fig. 10a) indicates that buoyancy flow and the bypassing of brine within the plume both strongly contribute to the early arrival of CO_2. This finding reiterates the value of a numerical model for interpreting field data. It also illustrates the difficulty of trying to define a simple performance measure such as average CO_2 saturation, which is needed for making capacity assessments of potential CO_2 geologic storage sites (Doughty et al. 2001; Hesse et al. 2006). The average CO_2 saturation within the plume primarily reflects two-phase flow behavior, and indicates the fraction of individual pores that are filled with CO_2. Theoretically it should be consistent with values inferred from laboratory studies. However the average CO_2 saturation over the entire formation is more relevant for capacity assessment, and if buoyancy flow (or heterogeneity) causes the CO_2 plume to avoid large fractions of the formation entirely, the formation-average saturation and the plume-average saturation will be quite different. Neither way of averaging is wrong per se, but care must be taken to use each average in the proper context.

Pressure-transient analysis

Downhole pressure was measured in both wells throughout the 10-day CO_2 injection period and for about 2 weeks thereafter (Benson and Doughty 2006; Hovorka et al. 2006). Compared to the 24-h interference test, this much longer monitoring period enables the hydrologic properties of more distant features of the fault block to be examined. For example, if the two fault-block boundaries nearest the wells (~600 m to the northwest and ~250 m to the southeast) are considered constant-pressure boundaries, which works for the interference test, modeled pressure increases

Table 5 Comparison between aqueous-phase tracer test and CO_2 arrival times

	Tracer test	CO_2 injection	Impact on CO_2 arrival time
Arrival at observation well	9 days	2 days	
Flow field	Doublet	Single well	3 times slower
Injection rate	50 gpm	40 gpm	20% slower
Phase conditions	Single-phase	Two-phase	Faster, bypass pore space containing other phase
Density contrast	None	1.5	Faster, buoyancy flow
Viscosity contrast	None	12	Faster, enhanced buoyancy flow
Density in situ	1,060 kg/m^3	~800 kg/m^3	20% faster

accompanying CO_2 injection are too small. In contrast, if the more distant salt-dome boundary (~1,200 m to the northeast) is considered a constant-pressure boundary, model pressure increases during CO_2 injection are about right, whereas a closed boundary there produces model pressure increases that are too large. Whether this boundary is closed or constant-pressure has no effect on the shorter interference test.

Several stoppages were planned for the injection period, so that pressure-transient analysis could be conducted under two-phase flow conditions. Additional short-term breaks in injection occurred due to operational problems. Pressure-transient responses under two-phase conditions are sensitive to relative permeability parameters, in addition to the intrinsic permeability and formation compressibility, which were inferred from the interference well test. Because only short breaks occur in the injection schedule, drainage is the dominant process occurring throughout the injection period, hence S_{lr} and m are the main parameters to infer. Figure 12 compares measured pressure change (ΔP) versus time to model ΔP obtained with the 8-m sand model using different parameter values. For the injection well, the coarse grid necessitates that a wellbore correction be made. At very early times, when the amount of injected CO_2 is small, single-phase liquid conditions control the pressure response and the correction (Peaceman 1978) yields a 0.5 bar increase. As more CO_2 enters the formation, the correction, which is directly

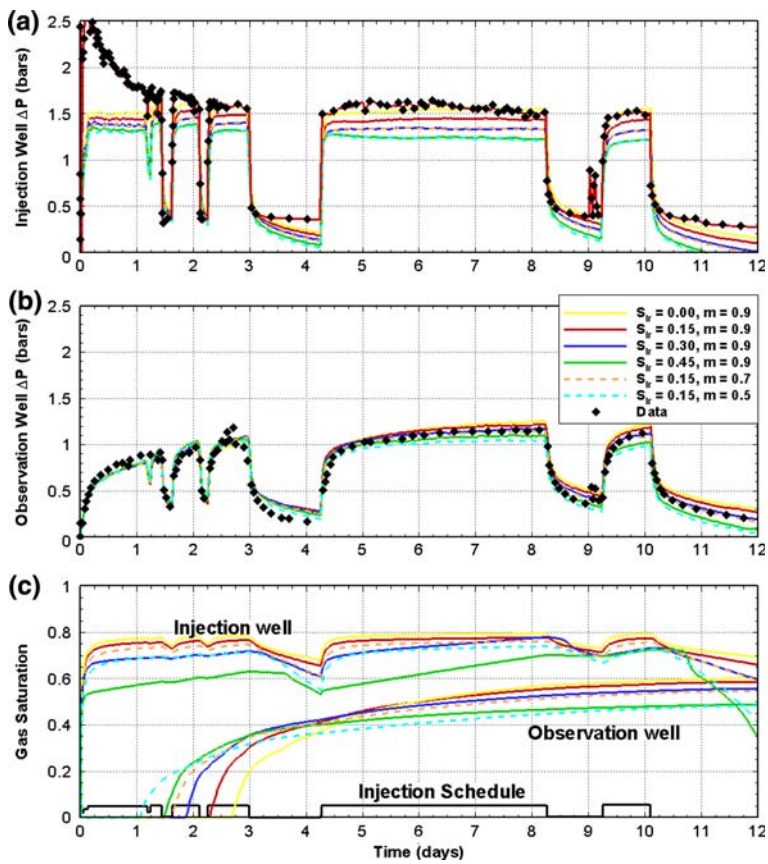

Fig. 12 Measured pressure transients (courtesy of Sally Benson, LBNL) and modeled pressure transients for the **a** injection well and **b** observation well, and **c** gas saturations at both wells during and immediately after CO_2 injection, for the 8-m sand model considering different two-phase flow parameters

proportional to the fluid viscosity at the well, becomes smaller, but the complication of a growing two-phase plume makes it impossible to quantify in a simple manner. Hence, comparisons between model and field data must remain qualitative for the injection well. It is clear from Fig. 12 that while S_{lr} and m affect the injection-well ΔP from the outset, they have very little impact on the observation-well ΔP until CO_2 fills the region surrounding the observation well, which occurs between four and ten days (compare Fig. 10a). Generally, ΔP decreases as S_{lr} increases and m decreases, consistent with the increase in total mobility that accompanies these parameter changes. The best match to observation-well ΔP is obtained for $S_{lr} = 0.30$, $m = 0.9$ and $S_{lr} = 0.15$, $m = 0.7$, but the sensitivity of the observation-well pressure transient data to S_{lr} and m is rather small, implying that other values of these parameters are also possible. There is little difference between ΔP values for the 5.5-m sand model and 8-m sand model, which is not surprising given that the two models produce identical pressure drawdown responses to the interference test.

Reservoir saturation tool

The wireline reservoir saturation tool (RST), developed by Schlumberger, uses pulsed neutron capture to determine changes in brine saturation as CO_2 displaces brine or vice versa (Sakurai et al. 2005; Hovorka et al. 2006). Figure 13 shows a time series of CO_2 saturation profiles derived from RST logs at the injection and observation wells, along with model results. Comparing depths at which CO_2 appears in the model to those from the RST logs provides valuable insights into geology, whereas comparing the magnitude of CO_2 saturation provides constraints on two-phase flow properties. Unfortunately, well workovers conducted at the end of the injection period changed conditions in the injection well so as to preclude analysis of the RST data at the depths of the perforations. There, $S_g = 0$ does not mean CO_2 is absent, just that no determination of S_g can be made.

At the injection well, Fig. 13a shows that CO_2 extends significantly below the perforated interval. This extension is reproduced by the 8-m sand model, but not by the 5.5-m sand model, where S_g drops to zero just below the perforated

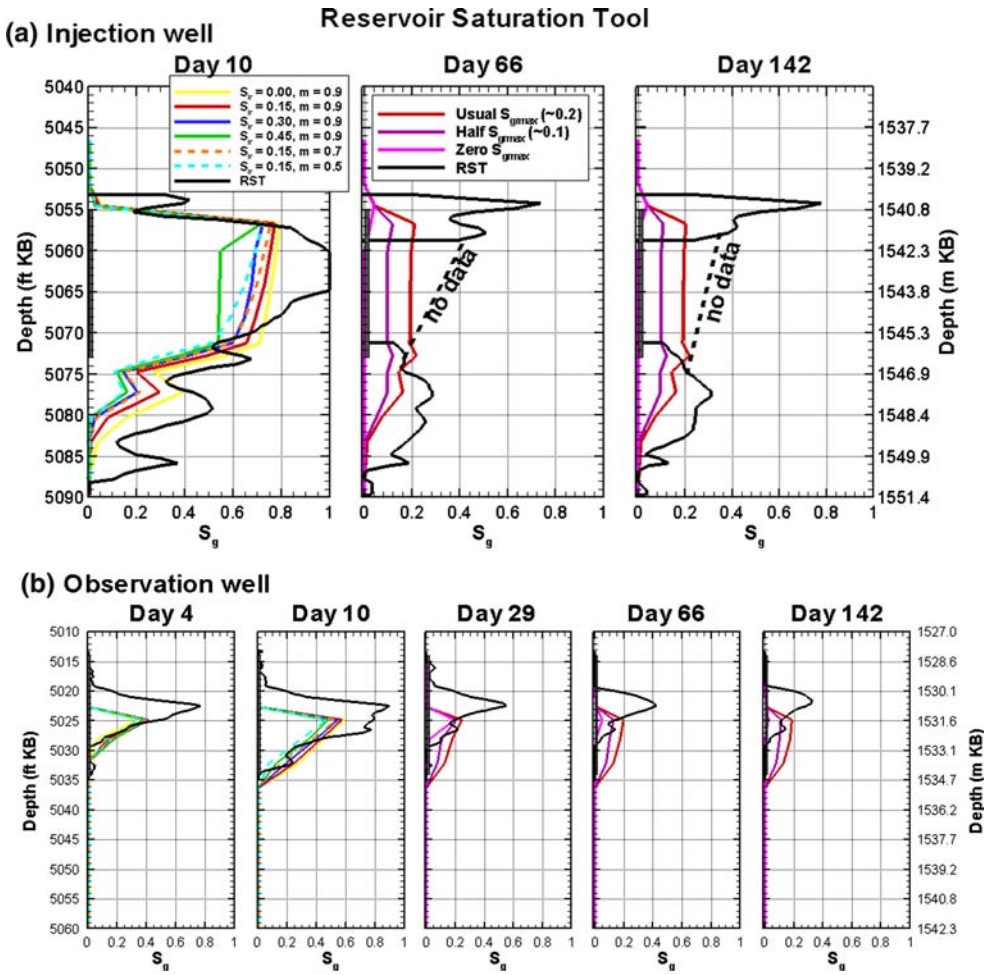

Fig. 13 CO_2 saturation profiles inferred from RST logs (courtesy of Shinichi Sakurai, TBEG) in the **a** injection well and **b** observation well. Model results for the 8-m sand model considering different two-phase flow parameters are also shown

interval (not shown). This finding supports the hypothesis underlying the 8-m sand model that the thin marker bed located just below the perforations does not have nearly as low a permeability as was inferred from well logs (Fig. 6b). At both wells, CO_2 extends almost 1 m shallower than predicted by the model, suggesting that a low-permeability layer identified just above the perforations in both wells may not be continuous, allowing CO_2 to move upward into an overlying sand. These findings are consistent with the large sand-layer thickness inferred from the single-phase tracer test, but only the CO_2 injection provides specific information about how this greater thickness may arise.

Reservoir saturation tool (RST) logs collected during the injection period (Fig. 13, day 4 and day 10) reflect a growing CO_2 plume, with drainage occurring throughout the plume, while those obtained during the subsequent rest period reflect the trailing edge of a migrating CO_2 plume, where imbibition occurs. Simulations results for the 8-m sand model for several values of S_{lr} and m (important during drainage, no effect during imbibition) and S_{grmax} (important during imbibition, no effect during drainage) are shown in Fig. 13. Figure 13 shows the expected dependence on S_{lr}, m, and S_{grmax}. During injection, as S_{lr} increases or m decreases, S_g decreases, as more brine is bypassed rather than being displaced by the invading CO_2, whereas during the subsequent rest period, different values of S_{lr} and m have no impact on the S_g profiles. In contrast, during injection S_{grmax} has no impact on the S_g profiles, whereas during the rest period the amount of CO_2 remaining in the region around the wells decreases dramatically as S_{grmax} is decreased.

The model trends as S_{lr}, m, and S_{grmax} vary appear reasonable, and support the use of a small value of S_{lr}, a large value of m, and a large value of S_{grmax} for modeling. However, all model S_g values are significantly smaller than the S_g values obtained from the RST logs, making it difficult to make quantitative decisions on the optimal values of parameters. The model results represent the average S_g over a 2-m wide grid block. An RST radius of influence smaller than 1 m could therefore account for some of the discrepancy, especially for the injection well, where conditions can change sharply close to the well. Another possibility is that the RST results include a significant contribution from what is in the wellbore as opposed to what is in the formation. The injection wellbore is certainly expected to be CO_2-filled during the injection period, and U-tube data indicate that the wellbore becomes CO_2-filled shortly after the CO_2 plume arrives at the observation well.

Crosswell seismic

Crosswell seismic data obtained using source and receiver strings in the observation well and injection well, respectively, were collected shortly before injection of CO_2 and again about 6 weeks after CO_2 injection ended (Daley et al. 2007). P-wave velocity depends on gas saturation S_g, so a difference tomogram of the seismic velocity before and after CO_2 injection provides an image of the free-phase CO_2 distribution in a vertical plane between the wells, as shown in Fig. 14a. A rock physics model for seismic velocity is needed to provide a quantitative relationship between velocity change and S_g. Ideally such a model would be site-specific, derived from core analysis and the relationship between well-log measurements of seismic velocity and well-log measurements of S_g, such as those obtained from the RST. Unfortunately, not all the requisite components for a rock physics model are available for the Frio formation C sand. However, a rock physics model calibrated to the Utsira Sand being used for the Sleipner CO_2 storage operation in the North Sea (Hoversten et al. 2003; Carcione et al. 2006) has been applied to the Frio formation C-sand velocity changes. This modeling suggests that 6 weeks after CO_2 injection ended, S_g in the vicinity of the injection well was approximately 20% and S_g near the observation well was approximately 10% (Daley et al. 2007). RST profiles collected during the CO_2 injection period for each well are shown along the sides of the tomogram, providing a consistency check on the seismic inversion. The crosswell seismic tomogram shows clearly that the inter-well region is heterogeneous, although

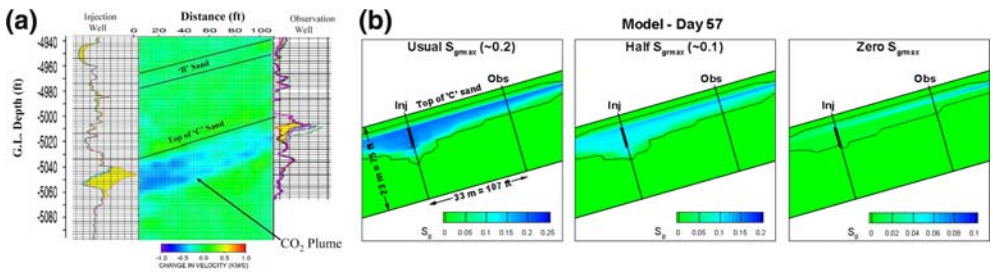

Fig. 14 **a** Crosswell seismic tomogram of the difference in P-wave velocity before and after CO_2 injection (Daley et al. 2007). **b** Modeled CO_2 distributions in the plane between the wells for the 8-m sand model considering different values of S_{grmax}. Note the different color scales for each case. The single *black contour line* shows $S_g = 0$, an indication of the historical maximum extent of the CO_2 plume

the resolution of the tomogram (1–5 m) precludes detailed interpretation of specific features.

Plots of the spatial distribution of CO_2 in the vertical plane between the injection and observation wells are shown in Fig. 14b for simulations using the 8-m sand model and three values of S_{grmax}. The model plume using the literature values of S_{grmax} (~0.2) matches the crosswell seismic tomogram best, with $S_g \sim 0.2$ near the injection well, and S_g decreasing and the plume becoming thinner as distance from the well increases. For the case with half S_{grmax}, the shape of the CO_2 plume is similar, but the modeled S_g is too low everywhere, and close examination shows that the maximum S_g does not occur at the injection well, but has migrated away from it. For the case with zero S_{grmax}, the plume migration is extreme and clearly not consistent with the field data. Hence, we infer that the original values of $S_{grmax} \sim 0.2$, which enable significant CO_2 mobility trapping, are optimal. The spatial distribution of CO_2 obtained with the 5.5-m sand model and $S_{grmax} \sim 0.2$ (not shown) is not dramatically different from that of the 8-m sand model, but the CO_2 plume is slightly thinner due to greater buoyancy flow, and hence does not match the seismic tomogram quite as well.

Vertical seismic profile

Vertical seismic profile (VSP) data were obtained by creating lines of explosions along the ground surface at three azimuthal directions around the injection well (NW, N, NE), and monitoring P-wave amplitude at the receiver string deployed in the injection well (Daley et al. 2007). VSP data were collected twice: once shortly before CO_2 injection, then again about 6 weeks after CO_2 injection ended. Figure 15 shows the change in P-wave amplitude before and after CO_2 injection, plotted as a function of offset from the injection well, for each direction, along with the corresponding model results for the 8-m sand model and three values of S_{grmax}. The resolution of the VSP data is about 10–30 m, whereas the model resolution varies from 5 m close to the wells to more than 100 m for the largest offsets shown. A quantitative relationship between VSP change in amplitude and CO_2 saturation is not known, so the vertical axes of the plot are adjusted to align these two quantities close to the injection well. For the usual S_{grmax} case, Fig. 15a shows good agreement between model and VSP in the updip direction (N), but the VSP indicates that the plume has moved farther than the model has predicted to the NE and NW. In fact, the plume has moved as far to the NW as it has to the N, suggesting that either local updip direction is not true north, or there is significant heterogeneity in the permeability distribution beyond the immediate vicinity of the wells, or the planar representation of a warped sand body becomes inaccurate

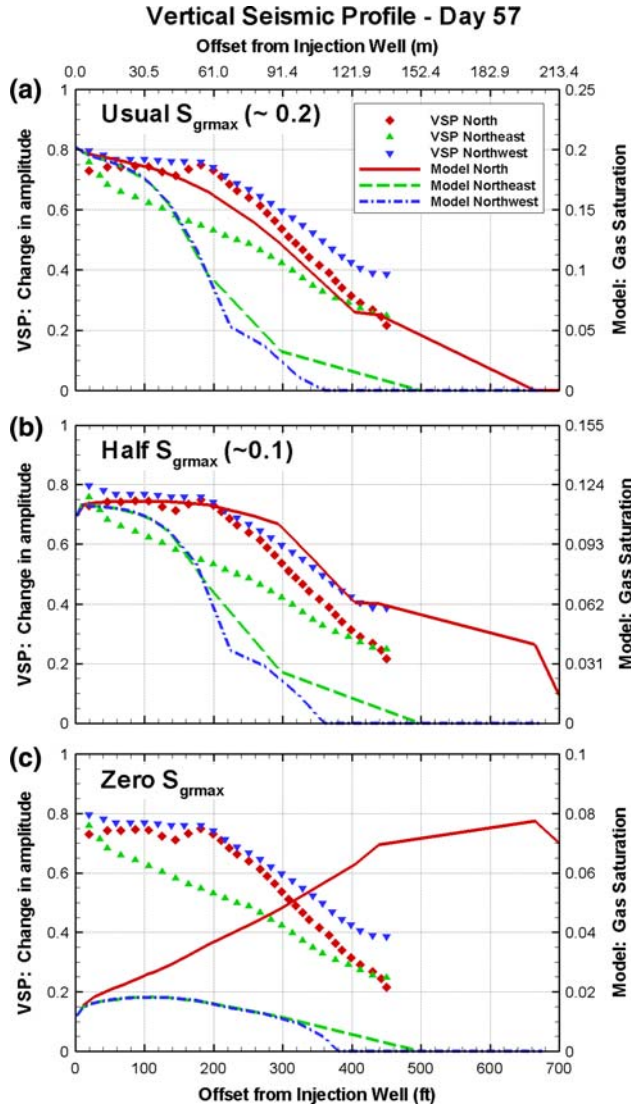

Fig. 15 VSP change in P-wave amplitude before and after CO_2 injection (Daley et al. 2007) and model results for far-field CO_2 distribution for the 8-m sand model considering different values of S_{grmax}

away from the wells. The non-smooth nature of the model profiles far from the injection well indicates the need for a more refined grid. Model results for the 5.5-m sand model do not differ significantly from those for the 8-m sand model.

For the half-S_{grmax} case, the model shows a little too much plume movement in the updip direction (N), while for the zero-S_{grmax} case, there is far too much plume movement updip, so we infer that the original values of $S_{grmax} \sim 0.2$, which allow less CO_2 to move updip, are optimal. Note that the modeled extent of the plume to the NE and NW is independent of S_{grmax}. Unlike other post-injection monitoring methods, VSP covers such a large spatial extent that it encompasses the entire CO_2 plume,

both the trailing edge around the wells, where imbibition is occurring, and the leading edge farther updip, where drainage is still occurring long after injection ceases. Hence, large-offset VSP results are also sensitive to drainage-controlling parameters S_{lr} and m. For a case with $S_{lr} = 0.3$ and $m = 0.9$, the leading edge of the CO_2 plume is about 10 m farther updip than is shown for the N profile in Fig. 15a.

Discussion

The interrelation between traditional site characterization and the CO_2 injection and monitoring employed at the Frio brine pilot proved very useful for analysis. For example, the single-phase interference well test provided basic information on hydrologic properties (permeability, compressibility, near-by boundary effects) that greatly expedited the more complicated multi-phase analysis required for the pressure transients obtained during CO_2 injection. Additionally, longer monitoring of pressure transients during CO_2 injection enabled more distant boundaries to be investigated.

In general, there is a natural progression of time scales moving from traditional site characterization (one to several days) to CO_2 injection and rest (several weeks to months) to monitoring during actual storage operations (many years) that corresponds to a natural increase in the spatial scale of the CO_2 plume as it grows and moves. The range of spatial scales investigated at the Frio brine pilot was large: a few centimeters for core studies, tens of centimeters for well logs, about 1 m for the RST, 30 m for crosswell seismic, 200 m for the VSP and interference-test pressure transients, and over one km for the CO_2-injection pressure transients. The numerical modeling was valuable for integrating and interpreting observations made on scales of a few meters and greater. Comparison with smaller-scale observations such as the injection-well pressure transients and RST profiles indicated that a higher-resolution model would be helpful for understanding near-wellbore effects. Another potential model improvement would be to apply the automated inversion techniques that have been developed for history matching (e.g., Finsterle 1999), to systematically optimize the model parameters to fit the field observations, instead of adjusting parameters by hand as was done here. Automated inverse techniques are particularly valuable when multiple parameters need to be estimated.

The information gleaned from CO_2 injection and monitoring can be broadly divided into two categories: improvements to the Frio formation C sand model and information on characteristic-curve parameters. Results in the first category are by their nature site specific, but the conditions that produce them, non-wetting phase CO_2 with a much lower density and viscosity than the native brine, are ubiquitous. Results in the second category should also be broadly applicable to other CO_2 geologic storage sites in saline formations.

Improvements to Frio formation C sand model

The fluorescein tracer test indicated that the high-permeability sand through which most fluid travels from the injection well to the observation well is 2.5-m thicker than that inferred from well logs, but did not provide any specific information on how the thickening occurs. The RST profiles for the injection well (Fig. 13a) suggest that the CO_2 plume extends almost 1 m above and several meters below the perforated interval, which was chosen to match the high-permeability zone identified in the well log (Fig. 6b). The RST profile for the observation well (Fig. 13b) confirms CO_2 arrival about 1 m shallower than predicted by the well logs, but because of buoyancy, no CO_2 arrives very far below the top of the high-permeability layer. The crosswell seismic tomogram (Fig. 14a) shows a CO_2 plume that is about 7.5 m thick at the injection well and thins toward the observation well. These findings support the choice of the 8-m sand model over the 5.5 m sand model. The next-generation model will increase permeability in the layers above the perforated interval as well, either over the entire model or locally. Some evidence for local variability is provided by the crosswell seismic tomogram (Fig. 14a), which shows a change in the character of the CO_2 distribution about half-way between the two wells.

The VSP data (Fig. 15) provide a powerful means of examining the evolution of the CO_2 plume beyond the immediate vicinity of the wells. Despite matching the updip migration adequately, the model fails to reproduce two other features of the VSP data. First, the CO_2 plume should extend just as far to the NW as it does to the N, suggesting a different local dip direction than currently employed by the model. Second, the lateral extent of the modeled plume is too small, suggesting a short-coming in the conceptualization of geological structure (e.g., the local dip magnitude may be smaller, lateral permeability anisotropy could exist, or the planar representation of a warped sand body becomes inaccurate). Because plume migration is largely a consequence of the buoyant flow of CO_2, these features would be difficult to ascertain from traditional site characterization methods.

The model changes described in the preceding paragraphs will improve on the current conceptual and numerical models of the C sand, and presumably result in improved matches to field data. However, there are other model shortcomings for which no specific modification has been envisioned. For example, it has not been possible so

far to find a single model that accurately matches the entire duration of the observation-well pressure transient for both the interference test and the CO_2 injection period. Although there are uncertainties in operational parameters (e.g., the mass injection rate during CO_2 injection) that could account for some of the discrepancy, the present understanding of distant boundary conditions and multi-phase flow effects is not yet complete.

Characteristic-curve parameters

During CO_2 injection periods, the entire CO_2 plume is undergoing drainage; that is, the non-wetting phase CO_2 is displacing the wetting-phase brine. After injection ends, the leading edge of a migrating CO_2 plume continues to drain, whereas the trailing edge of the plume is largely undergoing imbibition as wetting-phase brine replaces non-wetting-phase CO_2. Ideally, monitoring should be designed to cover both drainage and wetting processes, since they are controlled by different parameters. The drainage process, monitored at the Frio brine pilot via U-tube, early-time pressure transients and RST profiles, and large-offset VSP data, depends on S_{lr} and m, but is not sensitive to S_{grmax}. In contrast, the wetting process is not very sensitive to S_{lr} and m but depends strongly on S_{grmax}, thus late-time pressure transients and RST profiles, the crosswell seismic tomogram, and small-offset portions of the VSP data provide information on S_{grmax}.

These studies strongly support the notion that even for the very high-permeability Frio formation C sand (>2,000 md), S_{grmax} is well above zero, and even provides evidence that the original $S_{grmax} \sim 0.2$ is a better choice than the halved value of $S_{grmax} \sim 0.1$. The late-time RST profiles, the crosswell seismic tomogram, and the VSP data all show consistent results in this regard. Given the importance of a large value of S_{grmax} for trapping free-phase CO_2, and the fact that S_{grmax} increases as permeability decreases, this is an important finding for the overall potential for success of CO_2 geologic storage. The results also suggest that S_{lr} is small, consistent with petroleum-literature values (Holtz 2002). The U-tube results for CO_2 arrival at the observation well and pressure-transient analysis supports $S_{lr} = 0.15$, whereas the early-time observation-well RST suggests that S_{lr} is even smaller. A small value of S_{lr} means the CO_2 plume need not bypass so much liquid phase and can form a more compact plume in the subsurface. As one extrapolates from the very high permeabilities of the C sand to moderate permeabilities that may be more typical for CO_2 storage, S_{lr} is expected to increase.

Early in the CO_2 injection period, the simultaneous pressure observations in the injection well, which is surrounded by a two-phase mixture of CO_2 and brine, and the observation well, which is still surrounded by brine, potentially enable deconvolution of multi-phase flow effects, and improved determination of characteristic-curve parameters S_{lr} and m. Unfortunately, the present 3D numerical model is far too coarse (2-m resolution) to adequately resolve near-well effects at the injection well, making such analysis problematic. Studies with a high-resolution model are necessary. For short-time studies, one may be able to increase efficiency by using an RZ model, but for longer times, a 3D model is needed to represent the interplay of heterogeneity, buoyancy, and multi-phase effects.

Recall that these characteristic-curve parameter values are only meaningful in the context of the model in which they are used. Here the vertical grid spacing is on the order of 1 m and the lateral grid spacing in the vicinity of the wells is about 5 m. Hence, that is the scale for which these S_{grmax} and S_{lr} values are defined. They do not necessarily describe the fraction of an individual pore containing immobile gas or liquid, but rather the fraction of a meter-scale grid block, which likely includes unresolved heterogeneity. Similarly, a single-layer model of the C sand, which cannot resolve buoyancy flow to the top of the formation, requires a larger value of S_{lr} and a smaller value of m to match CO_2 arrival time and ΔP, to account for the bypassing of brine in the lower portion of the sand (Benson and Doughty 2006).

Concluding remarks

Well thought-out site characterization is essential for successful geologic storage of CO_2 because of the many physical processes impacting CO_2 plume evolution in the subsurface. At the Frio brine pilot, site characterization techniques such as geological mapping, geophysical imaging, well logging, core analyses, hydraulic well testing, and tracer testing were all valuable and formed the basis of initial site assessment. However, only through the injection and monitoring of CO_2 could the impact of the coupling between buoyancy flow, geologic heterogeneity, and history-dependent multi-phase flow effects truly be appreciated. Thus, the site-characterization process greatly benefited from the addition of CO_2 injection and monitoring. Moreover, development of a numerical model aided in the synthesis of geological, hydrological, and geophysical observations and provided a framework for understanding the coupled flow and transport processes occurring in the CO_2/brine system.

The advantages of using data collected during CO_2 injection to refine reservoir models are numerous. The obvious benefit of CO_2 injection is to provide information on multi-phase flow properties (primarily the residual phase saturations, below which CO_2 is trapped), which

cannot be obtained from traditional site-characterization techniques that examine single-phase conditions. Additionally, the low density and viscosity of CO_2 compared to brine causes the two components to flow through the subsurface differently, potentially revealing distinct features of the geology. Ultimately, to understand stored CO_2 behavior in the subsurface, there is no substitute for studying the movement of CO_2 directly.

It is humbling that even for the small-scale, very well studied, intensively monitored conditions of the research-oriented Frio brine pilot, there are still uncertainties in data interpretation. Even greater uncertainties are projected for full-scale CO_2 geologic storage projects, where economic constraints will limit the availability of data generated through expensive procedures such as tracer tests, fluid sampling, and crosswell seismic. With only one or two monitoring techniques it is generally not difficult to create a model that can reproduce field observations, making it easy to claim a full understanding of the geologic storage system. As different types of observations are added, matching them all becomes much more challenging, which may produce the feeling that understating of the system has actually decreased. In reality, an appreciation of ones level of ignorance has increased, which is generally a good first step for improving understanding. Despite the commercial pressures attendant to full-scale CO_2 geologic storage, it should be recognized that the coupled flow and transport processes that take place during CO_2 geologic storage can produce subtle and unintuitive effects that will affect the storage efficiency of a reservoir. It is valuable to investigate as many aspects of the system as possible, as embodied in the iterative approach of traditional site characterization and CO_2 injection presented here, to minimize uncertainty in an operational CO_2 storage project.

Acknowledgments Data provided by and stimulating discussions with members of the Frio brine pilot team, in particular Sue Hovorka, Mark Holtz, Shinichi Sakurai, and Joseph Yeh of University of Texas Bureau of Economic Geology (TBEG), Dan Collins of Sandia Technologies, and Tom Daley, and Sally Benson of Lawrence Berkeley National Laboratory (LBNL), are gratefully acknowledged, as are the reviews of this paper by Curt Oldenburg and Jens Birkholzer of LBNL and two anonymous reviewers. This work was supported by the Assistant Secretary for Fossil Energy, Office of Coal and Power Systems, through the National Energy Technology Laboratory, of the U.S. Department of Energy under Contract No. DE-AC02-05CH1123.

References

Ambrose WA, Lakshminarasimhan S, Holtz MH, Núñez-López V, Hovorka SD, Duncan I (2007) Geologic factors controlling CO_2 storage capacity and permanence—techniques and case studies based on experience with heterogeneity in oil and gas reservoirs applied to CO_2 storage. Environ Geol (this issue)

Bachu S, Bennion B (2007) Effects of in-situ conditions on relative permeability characteristics of CO_2-brine systems. Environ Geol (this issue)

Bachu S, Gunter WD, Perkins EH (1994) Aquifer disposal of CO_2: hydrodynamic and mineral trapping. Energy Convers Manage 35(4):269–279

Benson SM, Doughty C (2006) Estimation of field-scale relative permeability from pressure transient tests. Paper presented at CO2SC symposium, Lawrence Berkeley National Laboratory, Berkeley, CA, 20–22 March 2006

Carcione JM, Picotti S, Gei D, Rossi G (2006) Physics and seismic modeling for monitoring CO_2 storage. Pure Appl Geophys 163(1):175–207

Corey AT (1954) The interrelation between gas and oil relative permeabilities. Producers Monthly, November, pp 38–41

Daley TM, Myer LR, Peterson JE, Majer EL, Hoversten GM (2007) Time-lapse crosswell seismic and VSP monitoring of injected CO_2 in a brine aquifer. Environ Geol (this issue)

Doughty C (2007) Modeling geologic storage of carbon dioxide: comparison of hysteretic and non-hysteretic characteristic curves. Energy Convers Manage 48(6):1768–1781

Doughty C, Myer LR (2007) Scoping calculations on leakage of CO_2 in geologic storage: the impact of overburden permeability, phase trapping, and dissolution. In: McPherson B, Sundquist E (eds) Science and technology of carbon sequestration. American Geophysical Union, Washington DC (in press)

Doughty C, Pruess K, Benson SM, Hovorka SD, Knox PR, Green CT (2001) Capacity investigation of brine-bearing sands of the Frio Formation for geologic sequestration of CO_2. Paper presented at first national conference on carbon sequestration, National Energy Technology Laboratory, Washington DC, 14–17 May 2001

Doughty C, Pruess K, Benson SM (2003) Development of a well-testing program for a CO_2 sequestration pilot in a brine formation. Paper presented at second national conference on carbon sequestration, National Energy Technology Laboratory, Alexandria, VA, 5–8 May 2003

Doughty C, Pruess K, Benson SM, Freifeld BM, Gunter WD (2004) Hydrological and geochemical monitoring for a CO_2 sequestration pilot in a brine formation. Paper presented at third national conference on carbon sequestration, National Energy Technology Laboratory, Alexandria, VA, 3–6 May 2004

Ennis-King J, Paterson L (2005) Role of convective mixing in the long-term storage of carbon dioxide in deep saline formations (SPE 84344). Soc Petrol Eng J 10(3):349–356

Finsterle S (1999) ITOUGH2 user's guide. Lawrence Berkeley National Laboratory, Berkeley, CA, January, Rep LBNL-40040

Freifeld BM, Trautz RC (2006) Real-time quadrupole mass spectrometer analysis of gas in borehole fluid samples acquired using the U-tube sampling methodology. Geofluids 6:217–224

Freifeld BM, Doughty C, Trautz RC, Hovorka SD, Myer LR, Benson SM (2005a) The Frio brine pilot CO_2 sequestration test—comparison of field data and predicted results. Paper presented at the science and technology of carbon sequestration: methods and prospects for verification and assessment of sinks for anthropogenic carbon dioxide, AGU Chapman Conference, San Diego, CA, 16–20 January 2005

Freifeld BM, Trautz RC, Kharaka YK, Phelps TJ, Myer LR, Hovorka SD, Collins DJ (2005b) The U-tube: a novel system for acquiring borehole fluid samples from a deep geologic CO_2 sequestration experiment. J Geophys Res 110:B10203

Grove DB, Beetem WA (1971) Porosity and dispersion constant calculations for a fractured carbonate aquifer using the two well tracer method. Water Resour Res 7(1):128–134

Gunter WD, Perkins EH, McCann TJ (1993) Aquifer disposal of CO_2-rich gases: reaction design for added capacity. Energy Convers Manage 34(9–11):941–948

Gunter WD, Bachu S, Benson S (2004) The role of hydrogeological and geochemical trapping in sedimentary basins for secure geological storage of carbon dioxide. In: Baines SJ, Worden RH (eds) Geological storage of carbon dioxide. Geological Society, London, Special Publication 233, pp 129–145

Hantush MS, Jacob CE (1955) Non-steady radial flow in an infinite leaky aquifer. Trans Am Geophys Union 36(1):95–100

Hesse MA, Tchelepi HA, Orr FM Jr (2006) Scaling analysis of the migration of CO_2 in saline aquifers (SPE 102796). Paper presented at SPE annual technical conference and exhibition, San Antonio, Texas, 24–27 September 2006

Holtz MH (2002) Residual gas saturation to aquifer influx: a calculation method for 3-D computer reservoir model construction (SPE 75502). Paper presented at SPE gas technology symposium, Calgary, Alberta, Canada, 30 April–2 May 2002

Holtz MH (2005) Reservoir characterization applying residual gas saturation modeling, example from the Starfak T1 reservoir, middle Miocene Gulf of Mexico. MSc, University of Texas, Austin

Holtz MH, Doughty C, Yeh J, Hovorka SD (2004) Modeling of CO_2 saline aquifer sequestration and the effects of residual phase saturation. Paper presented at AAPG annual meeting, Dallas, 18–21 April 2004

Hovorka SD, Doughty C, Benson SM, Pruess K, Knox PR (2004) The impact of geological heterogeneity on CO_2 storage in brine formations: a case study from the Texas Gulf Coast. In: Baines SJ, Worden RH (eds) Geological storage of carbon dioxide. Geological Society, London, Special Publication 233, pp 147–163

Hovorka SD, Benson SM, Doughty C, Freifeld BM, Sakurai S, Daley TM, Kharaka YK, Holtz MH, Trautz RC, Nance HS, Meyer LR, Knauss KG (2006) Measuring permanence of CO_2 storage in saline formations—the Frio experiment. Environ Geosci 13(2):105–121

Hoversten GM, Gritto R, Washbourne J, Daley TM (2003) Pressure and fluid saturation prediction in a multicomponent reservoir, using combined seismic and electromagnetic imaging. Geophysics 68:1580–1591

IPCC (Intergovernmental Panel on Climate Change) (2005) In: Metz B, Davidson O, de Coninck HC, Loos M, Mayer LA (eds) Special report on carbon dioxide capture and storage. Cambridge University Press, Cambridge

Javandel I, Tsang C-F, Doughty C (1984) Groundwater transport: handbook of mathematical models. American Geophysical Union, Washington DC, Water Resources Monograph 10

Johnson JW Nitao JJ, Knauss KG (2004) Reactive transport modeling of CO_2 storage in saline aquifers to elucidate fundamental processes, trapping mechanisms and sequestration partitioning. In: Baines SJ, Worden RH (eds) Geological storage of carbon dioxide. Geological Society, London, Special Publication 233, pp 107–128

Kharaka YK, Hanor JS (2004) Deep fluid in the continents: I. Sedimentary basins. In: Treatise on geochemistry, vol 5. Surface and ground water, weathering, and soils. Elsevier-Pergamon, Oxford, pp 499–540

Kharaka YK, Cole DR, Hovorka SD, Gunter WD, Knauss KG, Freifeld BM (2006) Gas–water–rock interactions in Frio Formation following CO_2 injection: implications for the storage of greenhouse gases in sedimentary basins. Geology 34(7):577–580

Knox PR, Paine JG, Hovorka SD (2003) Environmental assessment: optimal geological environments for carbon dioxide disposal in brine formations (saline aquifers) in the United States—pilot experiment in the Frio Formation, Houston area: http://www.beg.utexas.edu/environqlty/co2seq/pubs_presentations/Frio_draftea4_03.pdf (cited 17 January 2007)

Kumar A, Ozah R, Noh M, Pope GA, Bryant S, Sepehrnoori K, Lake LW (2005) Reservoir simulation of CO_2 storage in deep saline aquifers (SPE 89343). Soc Petrol Eng J 10(3):336–348

Land CS (1968) Calculation of imbibition relative permeability for two- and three-phase flow from rock properties (SPE 1942). Soc Petrol Eng J June:149–156

Lindeberg E, Wessel-Berg D (1997) Vertical convection in an aquifer column under a gas cap of CO_2. Energy Convers Manage 38(Suppl):S229–S234

Mo S, Akervoll I (2005) Modeling long-term CO_2 storage in aquifer with a black-oil reservoir simulator (SPE 93951). Paper presented at SPE/EPA/DOE exploration and production environmental conference, Galveston, Texas, 7–9 March 2005

Oldenburg CM, Moridis GJ, Spycher N, Pruess K (2004) EOS7C version 1.0: TOUGH2 module for carbon dioxide or nitrogen in natural gas (methane) reservoirs. Lawrence Berkeley National Laboratory, Berkeley, CA, June, Rep LBNL-56589

Peaceman DW (1978) Interpretation of well-block pressures in numerical reservoir simulation (SPE 6893). Soc Petrol Eng J June:183–194

Pruess K, García J (2002) Multiphase flow dynamics during CO_2 disposal into saline aquifers. Environ Geol 42:282–295

Pruess K, Oldenburg C, Moridis G (1999) TOUGH2 user's guide, version 2.0. Lawrence Berkeley National Laboratory, Berkeley, CA, November, Rep LBNL-43134

Pruess K, Xu T, Apps J, García J (2003) Numerical modeling of aquifer disposal of CO_2 (SPE 83695). Soc Petrol Eng J 8(1):49–60

Riaz A, Hesse M, Tchelepi HA, Orr FM Jr (2006) Onset of convection in a gravitationally unstable diffusive boundary layer in porous media. J Fluid Mech 548:87–111

Sakurai S, Ramakrishnan TS, Boyd A, Mueller N, Hovorka SD (2005) Monitoring saturation changes of CO_2 sequestration: petrophysical support of the Frio brine pilot experiment. Paper presented at society of petrophysicists and well log analysts 46th annual logging symposium, New Orleans, LA, 26–29 June 2005

Smart PL, Laidlaw IMS (1977) An evaluation of some fluorescent dyes for water tracing. Water Resour Res 13(1):15–33

Spiteri EJ, Juanes R, Blunt MJ, Orr FM Jr (2005) Relative permeability hysteresis: trapping models and application to geological CO_2 sequestration (SPE 96448). Paper presented at 2005 SPE annual technical conference and exhibition, Dallas, Texas, 9–12 October 2005

Theis CV (1935) The relation between the lowering of the piezometric surface and the rate and duration of discharge of a well using ground-water storage. Trans Am Geophys Union 16:519–524

Trautz RC, Freifeld BM, Doughty C (2005) Comparison of single and multiphase tracer tests results from the Frio CO_2 pilot study, Dayton Texas. Paper presented at fourth annual conference on carbon capture and sequestration, National Environmental Technology Laboratory, Alexandria, VA, 2–5 May 2005

van der Meer LGH (1992) Investigations regarding the storage of carbon dioxide in aquifers in The Netherlands. Energy Convers Manage 33(5–8):611–618

van der Meer LGH (1996) Computer modelling of underground CO_2 storage. Energy Convers Manage 37(6–8):1155–1160

van Genuchten MTh (1980) A closed-form equation for predicting the hydraulic conductivity of unsaturated soils. Soil Sci Soc Am J 44(5):892–898